Physics Letters A 373 (2009) 3342–3349

Contents lists available at ScienceDirect

Physics Letters A

www.elsevier.com/locate/pla

Plume splitting in pico-second laser–material interaction under the influence of shock wave

Sobieslaw Gacek, Xinwei Wang *

Department of Mechanical Engineering, 2010 H. M. Black Engineering Building Iowa State University, Ames, IA 50011-2161, USA

ARTICLE INFO

Article history:
Received 28 April 2009
Received in revised form 11 July 2009
Accepted 17 July 2009
Available online 21 July 2009
Communicated by R. Wu

PACS:
81.16.-c
79.20.Ds
47.40.Nm
52.35.Tc

ABSTRACT

In this work, molecular dynamics simulations are conducted to study the physics of plume splitting in pico-second laser material interaction in background gas. The velocity distribution shows a clear split into two distinctive components. Detailed atom trajectory track reveals the behavior of atoms within the peaks and uncovers the mechanisms of peak formation. The observed plume velocity splitting emerges from two distinguished parts of the plume. The front peak of the plume is from the faster moving atoms and smaller particles during laser–material ablation. This region experiences strong constraint from the ambient gas and has substantial velocity attenuation. The second (rear) peak of the plume velocity originates from the larger and slower clusters in laser-material ablation. These larger clusters/particles experience very little constraint from the background, but are affected by the relaxation dynamics of plume and appear almost as a standing wave during the evolution. Density splitting only appears at the beginning of laser–material ablation and quickly disappears due to spread-out of the slower moving clusters. It is found that higher ambient pressure and stronger laser fluence favor earlier plume splitting.

1. Introduction

A wide spectrum of applications for pulsed lasers in material processing, thin film growth, and laser-assisted manufacturing has brought overwhelming interest to the field of laser–material interaction. The techniques are complicated and the dynamics of expanding laser ablation plume in background gas consists of many successive elaborated phenomena [1,2]. Over the last decade plume splitting in laser–material interaction has received much attention in literature and a preponderance of previous work has studied the phenomena both experimentally and theoretically. The most in-depth one that gives detailed accounts of the concerned effect is given by Geohegan et al. who provided first time compelling evidence of the plume splitting for yttrium in argon environment [3], and compared with results in several other systems, including Si/Ar, Si/He, YBCO/O_2 [4]. Furthermore, the authors interpreted the experimental results using dynamics calculations to exemplify this occurrence [5,6]. The nature of plume double-peaked arrangement in the background gas has been investigated by Bulgakov et al. [7–10] based on superconductor YBCO in oxygen and an endeavor of the respectable gas-dynamical modeling has been conducted. In prominent study by Harilal et al. the plume splitting has been observed also in carbon/helium system under different laser fluences [11], and the plume splitting effect was observed only in a particular pressure range in an Al/air system [12]. Moreover, the twin-peak distribution formation has been studied for different air pressures [13]. In recent years the work performed by Amoruso et al. [14–16] provides remarkable investigation of the clearly observed metallic plume splitting in a variety of gases such as helium, oxygen, argon and xenon for UV laser irradiation. The laser induced flow dynamics of ejected multicomponent LiF–C thin film at various laser fluence and different argon ambient pressures were analyzed in reference [17].

Various analytical techniques based on gas dynamics have been developed to study the laser ablation regime. These models provide somehow insufficient insight into the physical picture. To that subject more suitable appears to be the molecular dynamics or Monte Carlo simulation approach. One account of the strength of the atomistic investigation is to provide detailed explanation of nanoscale phenomena. A series of MD simulations on laser–material interaction have been conducted so far including work by Zhiglei et al. [18] and Wang's group [19–25]. Analysis from Itina et al.'s [26] numerical modeling based on the combined large-particle direct Monte Carlo simulation has provided compelling evidence on the existence of the double peaked character in Al/O_2 system. In that work the physics of plume splitting from the atomistic view were attempted to explain. This study represents further attempt to exemplify the fundamentals of plume splitting at atomistic level under the influence of shock wave. The designed model considers interaction with the background gas and takes into account the influence of the ambient pressure. This case is one of the most complicated because of the importance of the collective

* Corresponding author. Tel.: +1 515 294 2085; fax: +1 515 294 3261.
E-mail address: xwang3@iastate.edu (X. Wang).

0375-9601/$ – see front matter
doi:10.1016/j.physleta.2009.07.044

effects leading to the compression of both plume and gas and consequently to plume splitting.

2. Methodologies of simulation

The simulations are carried out based on our existing model, and detailed description has been given previously [19–22]. Briefly, the laser irradiates a free-standing argon film which is placed in a gas medium. Argon at 50 K is selected for film material for the simplicity of computation, and the gas shares similar properties as the target, such as molecular mass, but has a modified interatomic potential which considers only repulsive force between atoms. The film target is 108 nm long along the z axis (direction of laser incidence), below which there is a gas domain 271 nm long. In total, there are 337 500 atoms in a $32.5 \times 2.7 \times 3627$ (nm) ($x \times y \times z$) computational domain. Periodic boundary conditions are imposed to the boundaries in the x and y directions, and free boundary conditions to the boundaries in the z direction. We have adopted the Verlet algorithm for velocity integration in MD simulation [27]. Computational details along with parameter specifications are provided in our previous work [24].

A spatially uniform single laser pulse is applied on the film top surface. It has a temporal Gaussian distribution and fluence of 7 J/m^2. The laser pulse has 11.5 ps full width at half maximum (FWHM) and is peaked at 10 ps. The given laser fluence in the Letter is the one absorbed by the material, and no laser reflection (back scattering) is considered in our model. It is expected that if back scattering/reflection is considered, the behavior of atoms at the rear part of the plume will be affected to a limited extent. This is because the laser beam becomes already very weak at 20 ps. As will be discussed in Section 3, at this moment, the plume is at the very early stage of explosion. On the other hand, the plume splitting happens at a quite later time (500 ps) in our modeling. In the simulation, first the velocity of molecules is scaled up to 100 ps (time step: 25 fs) to make the sample reach 50 K. Then equilibrium calculation is conducted for another 100 ps to assure the disturbance caused by velocity scaling is eliminated. Towards the end of equilibration, the ambient gas reaches a pressure of 0.22 MPa. Finally after 200 ps, the laser beam heating is applied on the target top surface with volumetric absorption in the material. This incident laser beam is assumed to be absorbed exponentially with an artificial optical absorption depth $\tau = 5$ nm following the formula

$$dI/dz = -I(z)/\tau. \tag{1}$$

The laser energy within a time step (δt) is $E_1 = \delta t\, I A$, where A is the area of the target surface. This energy is absorbed exponentially inside the material by exciting the kinetic energy of atoms while keeping their momentum conserved. The laser energy absorbed within each layer (δz thickness) is

$$\Delta E = E_0\big(1 - \exp[-\delta z/\tau_0]\big), \tag{2}$$

where E_0 is the energy incident on one single layer in the z direction. Finally, laser beam absorption in the target is achieved by exciting the kinetic energy of atoms, and is accomplished by scaling the velocities of atoms by a factor which is expressed by [22]

$$\chi = \left\{1 + \Delta E\left[\frac{1}{2}\sum_{i=1}^{N} m_i\big((v_{i,1} - \bar{v}_1)^2 + (v_{i,2} - \bar{v}_2)^2 + (v_{i,3} - \bar{v}_3)^2\big)\right]^{-1}\right\}^{0.5}, \tag{3}$$

where $v_{i,j}$ and $\bar{v}_j$ ($j = 1, 2, 3$) are velocities of atom i and the average velocity in the x, y, and z directions for atoms in a layer normal to the laser beam. The new velocity, $v'_{i,j}$ of atom i is calculated as follows

$$v'_{i,j} = (v_{i,j} - \bar{v}_j) \cdot \chi + \bar{v}_j, \quad j = 1, 2, 3. \tag{4}$$

The invoked model also implements a special force eliminating procedure to terminate the reflected stress wave at the back side of the target [23–25].

3. Results and discussion

This work is focused on the physical process during the early stage of laser ablated plume propagation (up to 2 ns). In Fig. 1, the close-up of spatial behavior of the target material in the background gas at early stages of laser pulse duration up to 40 ps is presented. The pressure distribution is imposed to account for the plume formation and the interpretation of constraint effect by the background gas. The applied laser beam forces the target material to evaporate because its energy intensity exceeds the material ablation threshold. The highest pressure in the system (near 0.5 GPa) is generated inside the target material, about 10 nm under the top surface with distribution observable at 10 ps. That pressure peak propagates towards the opposite side of the target due to the stress development induced from laser action. When it reaches the left side, it disappears because of the force elimination boundary treatment implemented in this work. Nevertheless, the objective of this Letter is to focus on the dynamics of the ejected plume, where at 15 ps it already experiences violent phase change with rapid explosion. In following picoseconds the front of ablated material is characterized by the pressure peak due to the increasing constraint from augmented layers of compressing gas.

In Fig. 2 the velocity and density distributions are presented with superimposed atomic position of the front target region. At 5 ps the top material crystal structure is already destroyed and the atoms start to eject, propagating with significant gain in velocity. Density peak representing denser front region is already visible at 15 ps, which propagates with enormous velocity near 700 m/s. In later steps that trend is preserved and can be clearly observed at 40 ps.

It is important to notice very interesting occurrence visible starting from 10 ps namely the negative velocity, which moves to the backside of the target. It is induced by the local stress wave and is related to the dislocation of the local atoms under the influence of the stress [24]. It disappears when reaches the backside of the target because in the simulation a stress-absorbing boundary condition is applied on the left boundary by reducing the net velocity of atoms.

Ejected expanding plume leads to generation of an evidently strong shock wave composed of compressed adjacent gas near the target [24]. According to Zel'dovich and Raizer [28] shock wave formation is the result of a growing hydrodynamic interaction between the plume and the background gas and becomes important when the mass of the displaced gas is comparable to the mass of the plume. If the ablation rate is not high enough, the plume is too dilute for hydrodynamic effects to play a role, and no snowplow effect takes place. If the plume velocity is small, furthermore, shock wave is not formed because the plume expansion should be at least supersonic for the formation of shock wave [26]. In our simulation this favorable precondition is met at about 0.2 ns, where significant pressure increase is formed at the front of the compressed gas and shock wave generates (Fig. 3).

However, not the compelling shock wave characteristics, but primarily the intriguing pressure gradient across the plume material is the aspect of concern in this Letter. At initial expansion stages, the ejected material consists of very high pressure gradient in the front of the plume, which later on attenuates significantly due to the dissipation with the background gas (0.1 ns in Fig. 3).

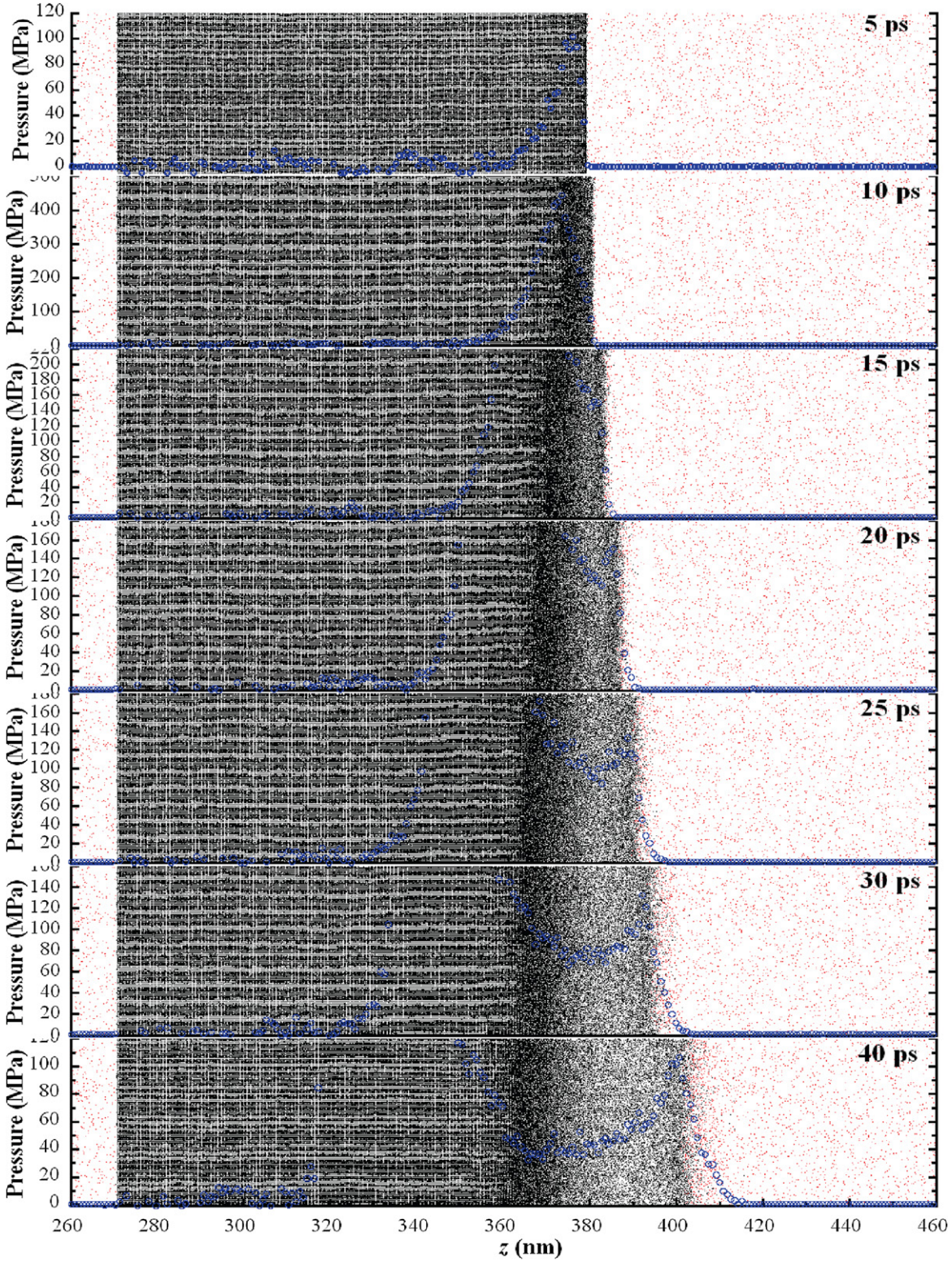

Fig. 1. Snapshots of atomic positions combined with the pressure distribution in the z direction up to 40 ps ($E = 7$ J/m^2, $\tau = 5$ nm, $P = 0.22$ MPa). Blue color: pressure; black dots: target atoms; red dots: ambient gas atoms. (For interpretation of the references to color in this figure legend, the reader is referred to the web version of this Letter.)

On the other hand the pressure gradient in the plume's tail region is not so steep and afterwards becomes rather uniform. Although the pressure carries lots of valuable information, the plume splitting explanation must be linked simultaneously with the velocity and density profiles. We will return to this pressure discussion later. Fig. 4 shows the target atoms transport in the two peak regions, which corresponds to temporal evolution dynamics of the plume up to 2 ns.

The plume splitting effect is perceptible with the formation of clear twin-peak behavior in the plume velocity profile (0.5–2 ns). Let us move to the elucidating of the reason of plume splitting whose configuration mechanism has to be recognized from the

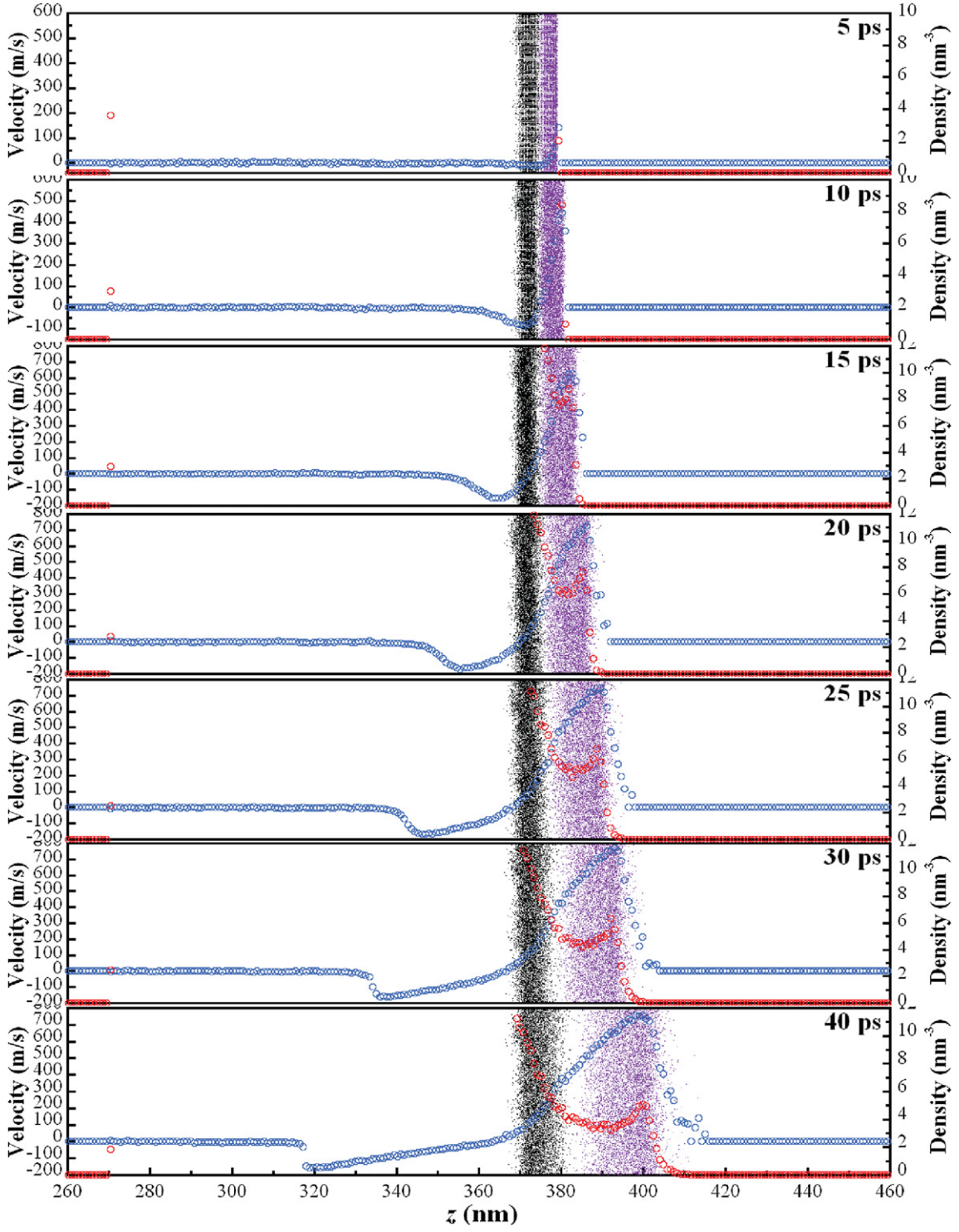

Fig. 2. Velocity and density distribution of the target material plume and the indication of the position of the plume two-peak propagation in the z direction up to 40 ps ($E = 7$ J/m^2, $\tau = 5$ nm, $P = 0.22$ MPa). Blue color: plume velocity; red color: plume density; violet dots: plume's first peak atoms position; black dots: plume's second peak atoms position. (For interpretation of the references to color in this figure legend, the reader is referred to the web version of this Letter.)

early time steps. The question is: Where do the atoms within the two peaks of velocity distribution come from? We track the history of these atoms, and find that the atoms in the front peak (Peak I) ($t = 1$ ns) come from the front of the plume. The second peak (Peak II) at 1 ns corresponds to atoms that are ejected having slower initial velocity. In Fig. 4 as well as in Fig. 2, the black dots represent the atoms flying out slowly at 0.2 ns, and the violet dots are the fast atoms in the front of the plume. The atoms in these two regions (region A and B) are marked in the inset in the figure at 0.2 ns in Fig. 3. The evolution of the velocity in the regions of interest can be explained inclusive of the pressure distribution shown in Fig. 3 in order to justify the formation of plume splitting. Upon laser irradiation, phase explosion will take place. The faster ejected particles (monomers, dimers, and smaller particles) quickly move out and interact with the ambient gas and feel the strong constraint from the ambience. Some of these plume species

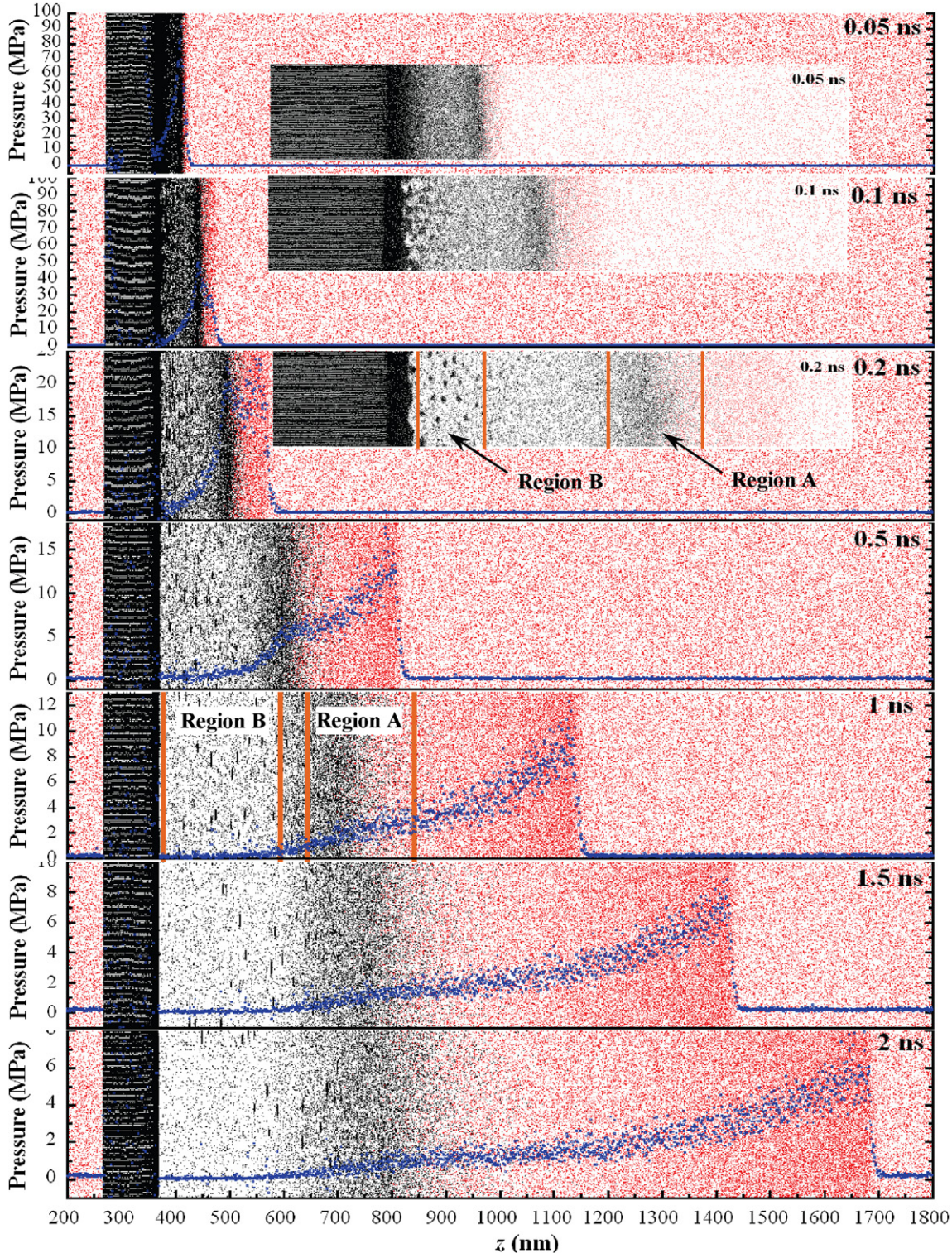

Fig. 3. Snapshots of atomic positions combined with the pressure distribution in the z direction between 0.05 and 2 ns ($E = 7$ J/m^2, $\tau = 5$ nm, $P = 0.22$ MPa). Blue color: pressure; black dots: target atoms; red dots: ambient gas atoms. (For interpretation of the references to color in this figure legend, the reader is referred to the web version of this Letter.)

are scattered in a backward direction during collisions with background gas molecules and interact with the incoming particles. These atoms form Region A (marked in Figs. 3 and 4). As shown in Fig. 3, in that zone, there is a very steep pressure gradient due to the strong constraint of the ambient gas. This large pressure gradient plays a critical role in slowing down the atoms in Region A. This velocity deceleration can be viewed clearly in Fig. 4. The velocity of atoms in the front of the plume zone reduces from the level around 800 m/s at 30 ps (Fig. 2) down to less than 100 m/s at 2 ns.

In the phase explosion vicinity section, at the early times (0.1, 0.2 ns), on the contrary, the larger particles have lower velocity and are left behind in the tail of the plume (Region B), as shown in Fig. 3. In that zone the pressure gradient is very small

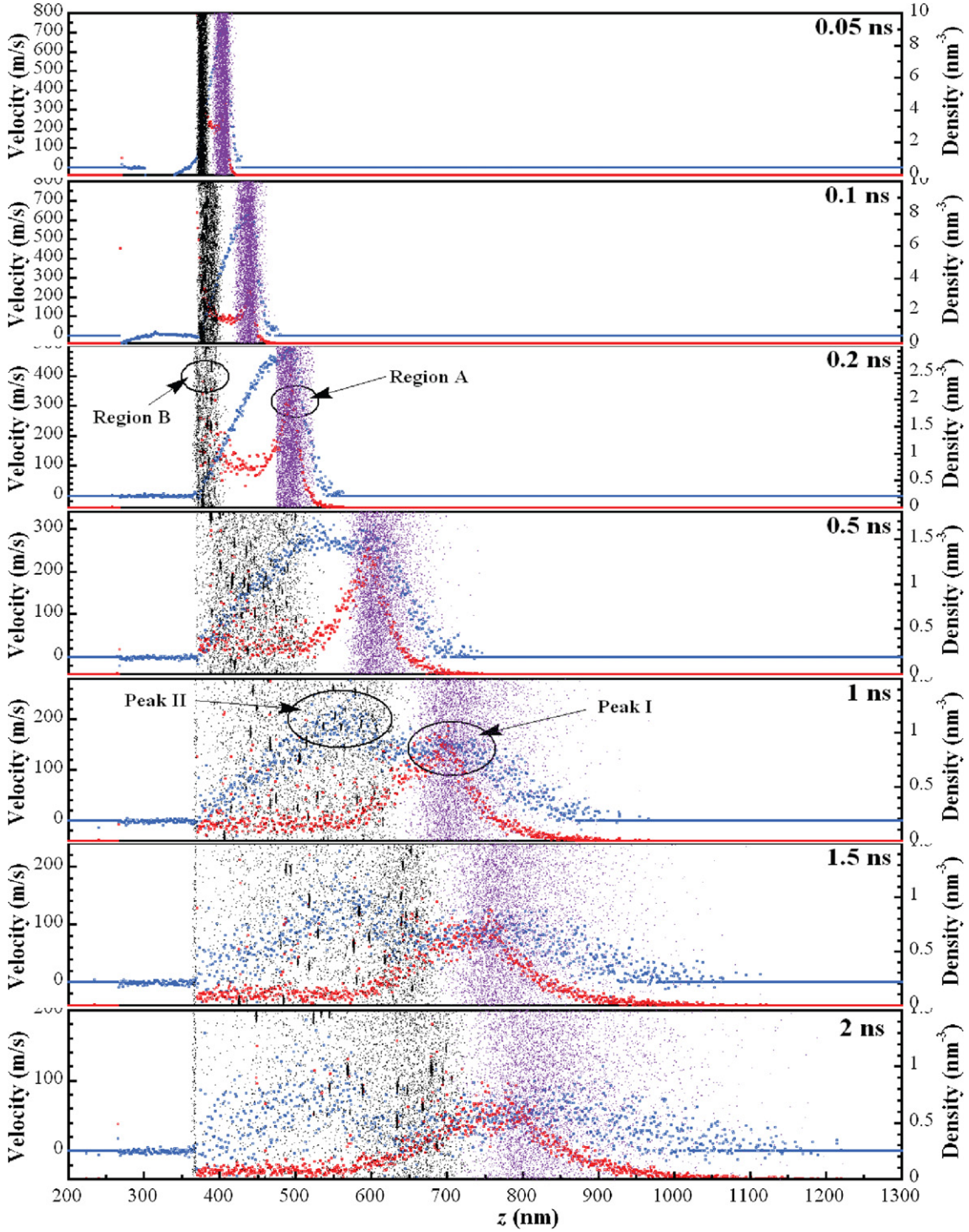

Fig. 4. Velocity and density distribution of the target material plume and the indication of the position of the plume two-peak propagation in the z direction between 0.05 and 2 ns ($E = 7$ J/m^2, $\tau = 5$ nm, $P = 0.22$ MPa). Blue color: plume velocity; red color: plume density; violet dots: plume's first peak atoms position; black dots: plume's second peak atoms position. (For interpretation of the references to color in this figure legend, the reader is referred to the web version of this Letter.)

(almost flat pressure distribution). Therefore, the atoms in Region B experience much less deceleration. In fact, since some particles still have phase change (vaporization) and their velocity is picking up from less than 100 m/s at 0.2 ns to more than 200 m/s at 0.5 ns. The deceleration of Region A and acceleration of Region B give strong contribution to the formation of plume splitting, which clearly emerges around 0.5 ns. At 2 ns, it is found most of the atoms in Region B have moved quite close to the ambient gas and their velocity reduces to less than 100 m/s.

These findings correspond well with experimental observations. According to Ref. [3] excited and ground-state Y^+ faster ions dominate the first peak, while excited and ground-state neutrals appear in the second, delayed distribution. Alike in Ref. [8] an increase in gas pressure is found to cause cluster formation in the second peak and the concentrations of plume mono- and polyoxides increase in first peak. In Ref. [9] mass spectrometric measurements demonstrate the front of the plume consists of various neutral species (atoms, small molecules such as YO, BaO) and the con-

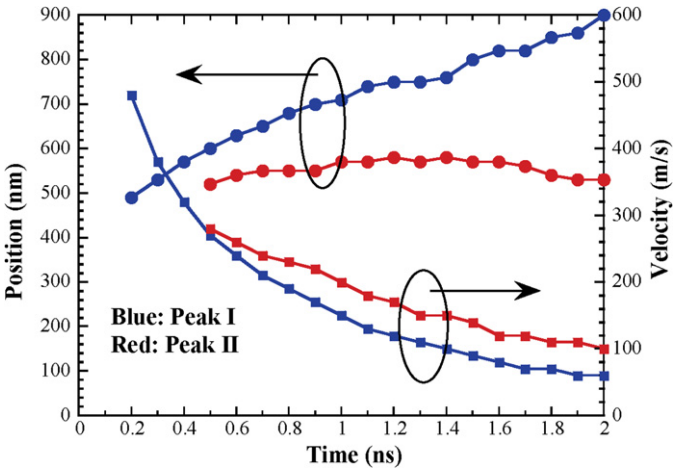

Fig. 5. Evolution of the position and the average atomic velocity within the two peaks. (For interpretation of the references to color in this figure, the reader is referred to the web version of this Letter.)

tent of molecular species and clusters (larger particles) is higher in the inner part of the plume since the slower atoms are involved predominantly in the conversion processes. Again in Ref. [10] it was claimed that ions were divided into fast (the high energetic, formed at an early stage of the plume expansion) and thermal components (the part of the ions being scattered and thermalized which forms the second slow peak and move together with the main body of the plume). In Refs. [12,13] it was observed that fast electrons and ions travel at the leading edge of the plume, where the ions located in the inner plume layers are accelerated much less due to hydrodynamic expansion (they remain much longer in the denser state, which is being subjected to strong recombination). In Ref. [15] it was confirmed that the ions and neutrals splits into two velocity populations. The faster component is due to particles that have been transmitted through the background gas almost without collisions, while the slower, delayed component is formed during the interaction between ablated species and background gas molecules. Finally, in Ref. [17] it was observed that energetic ions form the leading edge of the plume while majority of the materials propels from the substrate in the form of neutral vapor and move with much lower translational energy.

It is pertinent to notice that the double peak density formation of the plume can be observed at very early expansion times (less than 0.2 ns in Fig. 4 and Fig. 2). We believe that this occurrence is not just coincidence but it brings significant impact to the mechanism of the plume splitting. The leading density peak (Region A) characterizes the highest content of the atoms and is located in the front of the plume. During the plume expansion it retains its peak looking shape but 'snowplowing' of the background gas causes to diminish and broaden it. The other density peak initially being adjacent to the target surface (Region B), spreads over in the plume's shroud and exhibits sporadically spikes indicating appearance of nanoclusters (for example, at 2 ns in Fig. 4).

The plume velocity decay can also be viewed clearly in Fig. 5, where velocities of atoms in both peaks are presented against time. These curves represent the average atom velocity from regions belonging to each peak. As one can perceive the plume splitting is observable at 0.5 ns. Both velocity peaks decelerate very quickly from about 280 m/s at 0.5 ns to about 100 m/s and 50 m/s for peak II and peak I, respectively (2 ns). The moment when the split starts to appear can be also discerned from the propagation position of peak location (Fig. 5). While peak I moves out with time, peak II appears almost as a standing wave, showing little change of its location against time. This is clearly shown in Figs. 4 and 5. Such phenomenon holds on for about 1.5 ns during our simulation. Such standing-wave feature of Peak II is due to the strong relaxation of large particles/clusters and atoms in the plume. Similar velocity behavior has also been observed in the prominent computational study [26] at pressure of 70 Pa. The plume splitting has also been observed experimentally in the vacuum [10,17]. It seems that the phenomenon is more general in laser material interaction regime. It may indicate that the photomechanical effects with thermal desorption, melting, overheating and explosive boiling processes of the irradiated material plays important role in formation of fast atomic plume followed by a slower plume of aggregates.

Behavior of plume expansion dynamics is strongly dependent on the pressure and molecular weight of the ambient gas. Therefore dependence of plume splitting on background gas pressure and laser fluence has been studied as well in our simulation. In our work it is found the plume penetration depth into the background gas decreases when the ambient pressure is higher. When the ambient pressure increases, the plume expansion dynamics along with expansion velocities of the peaks are strongly affected by the interaction with the background gas and the plume stopping occurs at progressively earlier times and shorter distances from the target surface. The plume splitting is clearly observable but occurs much earlier and is much closer to the target surface under the ambient pressure 0.87 MPa, whereas for 0.051 MPa the plume with vague splitting occurs spatially at a longer distance from the target and generally later in time.

On the other hand elaborate experimental diagnostics such as emission and absorption spectroscopy, ion probe, as well as ICCD imaging have shown that at certain distance from the target the fraction of atoms from the plume that penetrate the surrounding gas as a freely expanding plume decreases strongly with the increasing gas pressure. This decrease is accompanied by a large enhancement of the slow component once a critical background gas pressure is reached, which leads to the plume splitting. This peculiar phenomenon was investigated in number of works. For example, for Y/Ar the plume splitting starts to be observable at 16.3 Pa [3]. For semiconductor ablated targets such as Si/Ar, the plume splitting is visible at 10.6 Pa [4] and at 16.6 Pa in Si/Ar (tested and visible up to 33.3 Pa) [6]. Moreover for Si in He environment the pressure must be increased beyond 20 Pa before two components become easily resolvable [4], alike in Ref. [6] where appears at 20 Pa (tested and visible up to 33.3 Pa). When high-temperature superconductor YBCO ablation was considered two distinct components are visible in O_2 at 10 Pa [4], and at 40 Pa clear split is apparent for YO, BaO, CuO species [7]. In Ref. [8] YBCO/O_2 system was tested in the pressure range of 0.0133–80 Pa. Up to 1.33 Pa the ambient oxygen has no considerable effect on the expansion while above 13.3 Pa it results in a twin peak behavior (at 25 Pa discernible and at 40 Pa clearly). Similar pressures are for YBCO/Ar [9]. On the other hand when graphite was ablated in air, splitting starts to appear at 5 Pa [10] (tested for the range of 0.1–100 Pa). For C_2 ablated in He (high purity polycrystalline graphite sample) splitting is already observable at 5 Pa [11]. When considering ablation of metals for Al/air, plume splitting and sharpening are observed only in a particular pressure range (around 20 Pa) [12]. Tested later in the range of 0.001 Pa–13.3 kPa confirmed split at 20 Pa [13]. For silver target, plume splitting is clearly observed in the heavy background gases, i.e. xenon (1.3 Pa), argon (6.2 Pa) and oxygen (6.5 Pa), while for the lighter helium it is not possible to discern two well separated ion components even at a pressure of few tenths of mbar (30 Pa) [14]. Similarly splitting starts for Ag/Ne at 45 Pa [16]. In $LaMnO_3/O_2$ system tested in range from vacuum to 100 Pa, lanthanum oxide and manganese oxide ion flux profiles split at 9 Pa [15]. For multicomponent LiF–C thin film deposited on a quartz substrate in argon, split appears at 1.5 Pa [17].

Generally, our results were found to be consistent with experimental work, to the point, that above certain pressure plume splitting occurs (above 0.051 MPa). Nevertheless, our system was designed to study the early stage shock wave dynamic, formation of the internal shock wave and plume's peculiar behavior rather than to recover an experimental condition. In here laser-argon crystal interaction was studied which is different from the commonly used materials such as aluminum, silicon or carbon and the laser type and wavelength has not been specified. However the simulations were framed in the way that laser beam can resemble generic situation of the laser material interaction.

The evolution from single-peaked to double-peaked plume has been investigated for two other laser fluences: 3 and 5 J/m^2. By increasing the irradiation level we observe that the plume propagation under higher fluences becomes more energetic and the plume splitting and plume sharpening is more noticeable. For irradiance in value of 3 J/m^2 the splitting effect is barely distinguishable and it occurs few tens of the picoseconds later than for 5 J/m^2 or 7 J/m^2. Under the fluence 5 J/m^2 the produced splitting of plume can be clearly noticed. Generally speaking, one can observe the apparent trend of the earlier occurrence of plume splitting when increasing the laser irradiance. To a large extent, since higher laser fluence results in more energetic particle formation, the velocity of those atoms and by that the peaks velocities are respectfully higher when increasing the fluence.

4. Conclusion

In this work, MD simulations were conducted to study the physics of plume splitting in laser material interaction up to 2 ns. Detailed atoms track allows us to specifically look into the behavior of atoms within the peaks and reveals the mechanisms of peak formation. The observed plume velocity splitting came from two distinguished parts of the plume. The front peak of the plume came from the faster moving atoms and smaller particles during laser–material ablation. This region experienced strong constraint from the ambient gas and had strong velocity attenuation. The second (rear) peak of the plume velocity originated from the larger clusters in laser–material ablation. These larger clusters/particles moved slower and experienced very little constraint, eventually picked up their velocity during the early evolution. At the very beginning of laser-ablation, two density peaks emerged and quickly disappeared due to the spread-out of the slower moving part. While the front peak propagated out against time, the second peak behaved as a standing wave and did not propagate but rather had a little trend towards the target surface. When the ambient pressure was increased, the plume splitting happened much earlier and occurred at a distance closer to the target surface. However, when the ambient pressure was reduced, the plume splitting became weak and barely visible. Under stronger laser fluence irradiation, the plume splitting will happen earlier.

Acknowledgements

Support for this work from the start-up fund of Iowa State University is gratefully acknowledged. Partial support for this work from NSF (CMS: 0457471) and MURI from ONR is gratefully acknowledged.

References

[1] D.B. Chrisey, G.K. Hubler (Eds.), Pulsed Laser Deposition of Thin Films, John Wiley & Sons, New York, 1994.
[2] R. Eason (Ed.), Pulsed Laser Deposition of Thin Films: Applications-Led Growth of Functional Materials, John Wiley & Sons, New Jersey, 2007.
[3] D.B. Geohegan, A.A. Puretzky, Appl. Phys. Lett. 67 (1995) 197.
[4] D.B. Geohegan, A.A. Puretzky, Appl. Surf. Sci. 96–98 (1996) 131.
[5] J.N. Leboeuf, K.R. Chen, J.M. Donato, D.B. Geohegan, C.L. Liu, A.A. Puretzky, R.F. Wood, Phys. Plasmas 3 (1996) 2203.
[6] R.F. Wood, K.R. Chen, J.N. Leboeuf, A.A. Puretzky, D.B. Geohegan, Phys. Rev. Lett. 79 (1997) 1571.
[7] A.V. Bulgakov, N.M. Bulgakova, J. Phys. D: Appl. Phys. 28 (1995) 1710.
[8] A.V. Bulgakov, M.R. Predtechensky, A.P. Mayorov, Appl. Surf. Sci. 96–98 (1996) 159.
[9] A.V. Bulgakov, N.M. Bulgakova, J. Phys. D: Appl. Phys. 31 (1998) 693.
[10] N.M. Bulgakova, A.V. Bulgakov, O.F. Bobrenok, Phys. Rev. E 62 (2000) 5624.
[11] S.S. Harilal, Appl. Surf. Sci. 172 (2001) 103.
[12] S.S. Harilal, C.V. Bindhu, M.S. Tillack, F. Najmabadi, A.C. Gaeris, J. Phys. D: Appl. Phys. 35 (2002) 2935.
[13] S.S. Harilal, C.V. Bindhu, M.S. Tillack, F. Najmabadi, A.C. Gaeris, J. Appl. Phys. 93 (2003) 2380.
[14] S. Amoruso, B. Toftmann, J. Schou, Appl. Surf. Sci. 248 (2005) 323.
[15] S. Amoruso, A. Sambri, M. Vitiello, X. Wang, Appl. Surf. Sci. 252 (2006) 4712.
[16] S. Amoruso, J. Schou, J.G. Lunney, Europhys. Lett. 76 (2006) 436.
[17] R.K. Singh, A. Kumar, IEEE Trans. Plasma Sci. 35 (2007) 1717.
[18] L.V. Zhigilei, E. Leveugle, B.J. Garrison, Y.G. Yingling, M.I. Zeifman, Chem. Rev. 103 (2003) 321.
[19] X. Wang, X. Xu, ASME J. Heat Transfer 124 (2002) 265.
[20] X. Wang, X. Xu, Int. J. Heat Transfer 46 (2003) 45.
[21] X. Wang, X. Xu, ASME J. Heat Transfer 125 (2003) 1147.
[22] X. Wang, J. Phys. D: Appl. Phys. 38 (2005) 1805.
[23] L. Zhang, X. Wang, Jpn. J. Appl. Phys. 47 (2008) 964.
[24] S. Gacek, X. Wang, Appl. Phys. A 94 (2009) 675.
[25] S. Gacek, X. Wang, J. Appl. Phys. Commun. 104 (2008) 126101.
[26] T.E. Itina, J. Hermann, P. Delaporte, M. Sentis, Phys. Rev. E 66 (2002) 066406.
[27] M.P. Allen, D.J. Tildesley, Computer Simulation of Liquids, Clarendon Press, Oxford, 1987.
[28] Y.R. Zel'dovich, Y.P. Raizer, in: W.D. Hayes, R.F. Probstein (Eds.), Physics of Shock Waves and High-Temperature Hydrodynamic Phenomena, Academic Press, New York and London, 2001.